Dielectronic recombination process in laser-produced tantalum plasmas

C. Bauche-Arnoult, J. Bauche, E. Luc-Koenig, and J.-F. Wyart
Laboratoire Aimé Cotton, CNRS II, Bâtiment 505, 91405 Orsay, France

R. M. More,* C. Chenais-Popovics, J.-C. Gauthier, J.-P. Geindre, and N. Tragin
Laboratoire d'Utilisation des Lasers Intenses et Laboratorie de Physique des Milieux Ionisés, Ecole Polytechnique, 91128 Palaiseau, France

(Received 4 August 1988)

The $3d$-$4f$ and $3d$-$5f$ emission patterns occurring between 4.5 and 6.5 Å in the spectra of laser-produced plasmas of highly ionized tantalum are studied, and the pseudocontinuum which underlies the former is interpreted. For the transition subarrays suspected to be responsible for the pseudocontinuum, the average wavelengths and widths are computed *ab initio* in the formalism of spin-orbit-split arrays; these subarrays are proven to cover a continuous band of wavelengths. For their intensities, the dielectronic recombination (DR) process populates efficiently the upper configurations, which, in most cases, lie above the ionization levels. The autoionization and radiative-transition probabilities, and the DR coefficients, are computed *ab initio*, in the form of averages for whole configurations or subconfigurations of Cu-like tantalum. The compact formulas for these averages are valid in intermediate coupling, avoiding any diagonalization. All the needed radial integrals are computed by means of a relativistic parametric potential central-field code.

I. INTRODUCTION

Many spectra of highly ionized heavy atoms in laser-produced plasmas are now available for the elements rare earths through lead, in the wavelength range 3–10 Å (see Ref. 1 and references therein). In these spectra, the lines emitted by the Ni-like species, with ground-state configuration $KL3s^23p^63d^{10}$ (K and L are closed shells $n=1$ and 2) are among the most intense. They correspond to the electronic transitions $3d$-np, $3d$-nf, $3p$-ns, $3p$-nd, and $3s$-np.

The $3d$-$4f$ transition is predominant, with only two very strong lines, denoted $3d^{10}$-$3d^9_{3/2}4f_{5/2}$ and $3d^{10}$-$3d^9_{5/2}4f_{7/2}$ (the third one, $3d^{10}$-$3d^9_{5/2}4f_{5/2}$, is predicted to be very weak and is not observed). Each of the former two lines is associated with satellite-emission features, corresponding to the transition arrays $3d^9$-$3d^84f$ (Co-like array at shorter wavelengths), $3d^{10}nl$-$3d^94fnl$, $3d^{10}nln'l'$-$3d^94fnln'l'$, $3d^{10}nln'l'n''l''$-$3d^94fnln'l'n''l''$, etc. (Cu-, Zn-, Ga-like arrays, etc., at longer wavelengths).

Detailed analyses of the spectra have been performed on the analogous $3d$-$5f$ transitions in the case of Ta,[2] Au,[3] W.[4] Because the lines are unresolved, and the spin-orbit interactions are very large, the calculations were made in the spin-orbit-split-array (SOSA) formalism,[5] yielding the average wavelengths and full widths at half maximum (FWHM) of the different *transition subarrays,* without any energy matrix building and diagonalization. Actually, for a given species (Cu-, Zn-, and Ga-like, etc.) various subarrays may coalesce in a single peak, and peaks from different species may blend. Nevertheless, the calculated $3d$-$5f$ features are in very good agreement with experiment.

Such a study has been extended up to $n=9$ for $3d$-nf, $n=6$ for $3p$-nd, and $n=5$ for $3s$-np, for several elements from Ta to Pb.[1] All the transition arrays, except $3d$-$4f$, exhibit well-separated easy to identify peaks, even if some of them are blended with other features. On the contrary, the $3d$-$4f$ peaks often appear superimposed upon a sort of pseudocontinuum, for example, in Gd,[6] Au,[7] Tm, Yb, Hf, and Ta (Ref. 8) spectra. Moreover, it is noteworthy that the shape of the pattern may strongly depend on the plasma parameters, as is shown in Fig. 1. It seemed up to now that the SOSA formalism, successful in many cases, was insufficient for describing fully the $3d$-$4f$ transition region.[8]

The aim of the present paper is to propose an interpretation of this difference between the $3d$-$4f$ and other transition patterns. In Sec. II the experimental techniques used to obtain the x-ray plasma are described. In Sec. III it is shown that many upper configurations are likely to decay through unresolved transition arrays hitherto overlooked, and that some of them can be definitely identified in experimental spectra. In Sec. IV the phenomenon of dielectronic recombination is proven quantitatively to be efficient enough for populating the relevant upper configurations. For that purpose, the dielectronic-recombination process is computed for configurations and subconfigurations instead of individual levels. The comparison with experiment is reported in Sec. V.

II. EXPERIMENTAL TECHNIQUES

The experiments were performed at the LULI (Laboratorie d'Utilisation des Lasers Intenses) laser facility, using a single beam of a frequency-doubled 1.05-μm phosphate-glass laser focused by a 250-mm focal-length lens onto planar tantalum targets. The pulse length was 600 ps, and the average laser flux was in the range 10^{13}–5×10^{14} W/cm^2. In recent experiments, the spectra were obtained by a time-integrating, space-resolving crys-

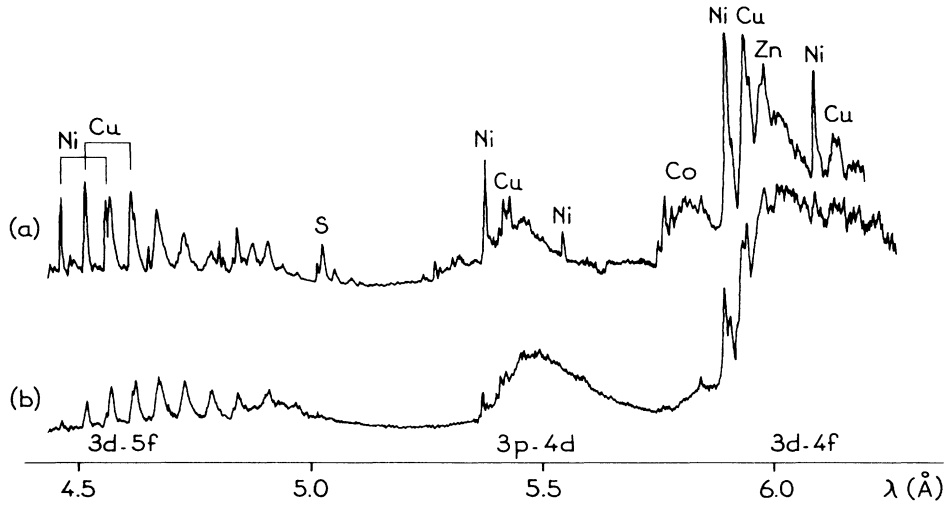

FIG. 1. Spectra of tantalum in a laser-produced plasma, in the range 4.5–6.0 Å. (a) High-irradiance laser plasma (3×10^{14} W/cm^2). (b) Low-irradiance laser plasma (3×10^{13} W/cm^2). In (b), the Ni- and Cu-like ionic species are depleted and a quasicontinuum dominates the long-wavelength $3d$-$4f$ range. S, sulphur lines used for calibration.

tal spectrometer viewing the target with an angle of 7° from the target plane. A spatial resolution of 10 μm was obtained by using an imaging knife-edge technique.[9] Data analysis and wavelength calibration techniques have been described elsewhere.[7]

Figures 1(a) and 1(b) show two tantalum spectra covering the range 4.5–6 Å, obtained at 3×10^{14} and 3×10^{13} W/cm^2 laser irradiances. They clearly show the emission of $3d$-$5f$, $3p$-$4d$, and $3d$-$4f$ transition subarrays. Unfortunately, these spectra are time and space integrated, and it is rather difficult to estimate the plasma parameters in both conditions. However, the different ratios of nickel-like to copperlike emissions suggest that the electron temperature is smaller at low laser intensity. More evidently, the intensity ratio of the peaks to the continuum is very much increased at high irradiance.

Figure 2 shows an expanded region around the $3d$-$4f$ subarrays, in another laser shot taken at 5×10^{14} W/cm^2. This spectrum is space resolved.

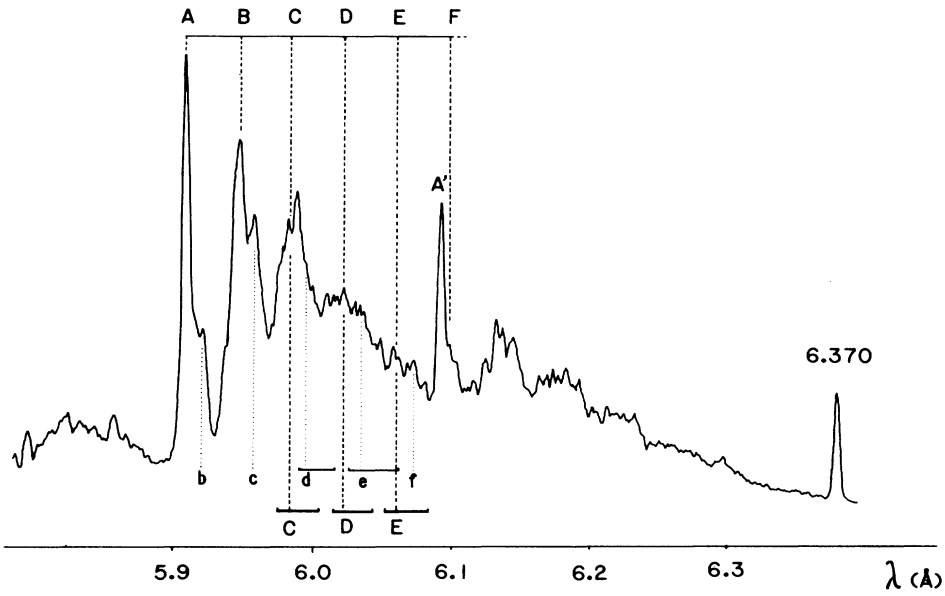

FIG. 2. $3d$-$4f$ transition range in the tantalum spectrum. A and A', Ta^{45+} (Ni-like) $3d_{3/2}$-$4f_{5/2}$ and $3d_{5/2}$-$4f_{7/2}$ transitions. B, C, D, E, . . . axes of the Cu-, Zn-, Ga-, and Ge-like tantalum emission peaks, corresponding to the transition $3d^{10}$-$3d^9_{3/2}4f_{5/2}$ plus one, two, three, four, . . . $4l$ spectator electrons added, respectively. b, c, d, e, . . . same ionic species as above but, among the spectator electrons, one belongs to the $n=5$ shell. The horizontal bars represent the spread of the positions of the different subarrays composing the peaks. The line at 6.370 Å corresponds to the Ni-like $3p_{1/2}$-$4s$ transition.

III. WAVE NUMBERS OF SUBCONFIGURATIONS AND SUBARRAYS

As is apparent in Fig. 2, the $3d$-$4f$ experimental pattern can be roughly divided into three ranges as follows.

(i) On the short-wavelength side, a weak, broad, nearly structureless feature, which is a part of the Co-like $3d^9$-$3d^8 4f$ (Ta^{46+}). This array brings small contributions to the ranges (ii) and (iii), together with Ni-like satellites $3d^9 nl$-$3d^8 4fnl$, etc., but they cannot be identified. They are neglected in the following.

(ii) At $\lambda = 5.907$ Å, the strong Ni-like $3d^{10}$-$3d^9_{3/2}4f_{5/2}$ line (Ta^{45+}), and, at longer wavelengths, its Cu-, Zn-, Ga-, and Ge-like satellite subarrays (Ta^{44+}-Ta^{41+}), corresponding to the addition of one, two, three, and four spectator electrons.

(iii) At $\lambda = 6.092$ Å, the Ni-like $3d^{10}$-$3d^9_{5/2}4f_{7/2}$ line, and, at longer wavelengths, its Cu-, Zn-, Ga-, and Ge-like satellite subarrays, like in range (ii).

In the following, only range (ii) is studied in detail, because its intensity is larger and it is better resolved. The analogous range (iii) is shifted by about -50 eV (0.185 Å), and overlaps the long-wavelength "tail" of range (ii), i.e., the As-like subarrays, etc. Thus the excited levels relevant to the emission in range (ii) must first be defined and located.

A. Upper subconfigurations

Most of the upper configurations responsible for the emission in the 3–10-Å wavelength range of the Ta spectrum lie above the relevant ionization limit. In Fig. 3, the computed energies of some of these configurations associated with the $3d$-nf transitions are plotted, for $n \geq 4$, in the Ni-, Cu-, and Zn-like ions. Each long horizontal bar represents the total electronic energy of the ground-state level of the corresponding ion. The short horizontal segments represent the calculated average energies for the following subconfigurations (hereafter, $3d^9 4f$ stands for $3d^9_{3/2}4f_{5/2}$.

(i) For the Ni-like ion (left column), $3d^9 n'f$ ($n' = 4$–9), the metastable $3d^9 4s$ configuration, and the ionization limit (the ground-state level of the Co-like ion).

(ii) For the Cu-like ion (center column), on the left $3d^9 4fnl$ ($n = 4$–7; for $n = 5$–7, only the spreads are plotted) and the lowest excited configuration $3d^{10}4p$, in the center the spreads of the configurations $3d^9 n'f4l$ ($n' = 5$–9) for $l = 0$–3, and on the right the spread of $3d^9 5f5l$.

(iii) For the Zn-like ion (right column), $3d^9 4f4s4l$ and $3d^9 4f4s5l$, with dashed lines the spreads of $3d^9 4f4l4l'$, $3d^9 4f4l5l'$, and $3d^9 4f5l5l'$ (limited to $l, l' \leq 2$, i.e., to configurations decaying through $3d$-$4f$ transitions towards bound configurations) and the lowest excited configuration $3d^{10}4s4p$.

It must be added that, for the upper configurations which emit towards the relevant lower configuration, the plotted average energy is that of the corresponding *emissive zone*.[10,5] For example, this average energy is larger than that of the whole configuration by 13.8 eV for the $3d$-$4f$, and 5.5 eV for the $3d$-$5f$ emissions. The ionization potentials are, respectively, 2315, 2254, 2050, and 1995 eV for the Cu-, Zn-, Ga-, Ge-like ions.

All the calculations presented here have been made by means of the relativistic central-field *ab initio* method.[11,12] The wavelengths of the $3d_{3/2}$-$4f_{5/2}$ transitions have been shifted by 0.015 Å to fit the experimental values. This is due to configuration interaction between the subconfigurations $3d^9_j 4f_{j'}$. In the $3d$-$5f$ transitions, this effect is completely negligible.

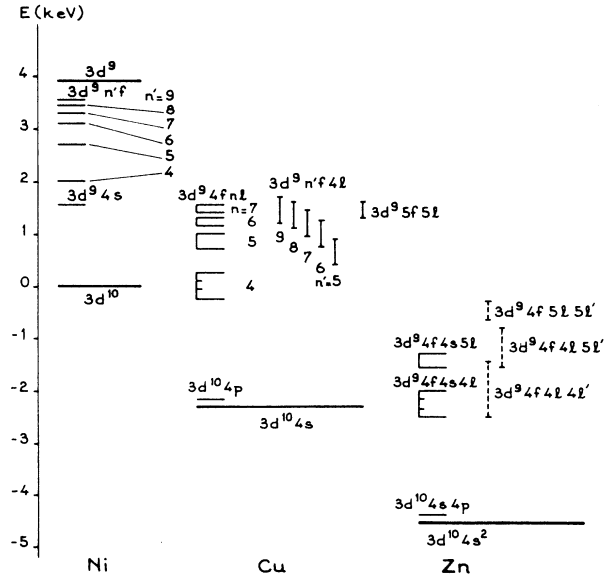

FIG. 3. Positions of some configurations involved in the transitions under study in the Ni-, Cu-, and Zn-like tantalum spectra.

B. Spin-orbit- split arrays

In the present approximation, all the lines originating from an upper subconfiguration (in j-j coupling) are considered as contributing to one unresolved subarray; the array splits into subarrays, whose FWHM's can be computed by means of compact formulas.[5] An example of moderate complexity is that of the Cu-like $3d^{10}4l$-$3d^9 4f4l$ arrays. Only the $3d_{3/2}$-$4f_{5/2}$ transitions are considered here. Therefore there appear seven subarrays, associated with the different l and j values of the spectator electron, which are denoted $3d^{10}4l_j$-$(3d^9)_{3/2}4f_{5/2}4l_j$ and are listed, with their calculated FWHM, in the left part of Table I. It is noteworthy that all seven subarrays have nearly the same average energy (or wavenumber), namely, 5.947 ± 0.004 Å, a result which is studied in the Appendix.

In the Zn-like $3d^{10}4l_j 4l'_j$-$3d^9_{3/2}4f_{5/2}4l_j 4l'_{j'}$ case there appear 28 subarrays, whose calculated average wavelengths and FWHM's are listed in the right part of Table I. These subarrays sum up into just one peak, like the Cu subarrays, but with a larger width.

For the arrays with more spectator electrons, namely in the Ga-, Ge-, and As-like spectra, the number of possible subarrays increases very rapidly. The patterns

TABLE I. Mean wavelengths and widths of the subarrays composing the Cu- and Zn-like peaks $3d_{3/2}$-$4f_{5/2}$ (satellite $4l$). All entries are in Å, except the FWHM (numbers in parentheses), which are in mÅ. These widths are calculated in the SOSA formalism (Ref. 5). The instrumental width is not taken into account. The extremal numbers are underlined.

Cu-like ions $3d^{10}nl_j$-$3d^9_{3/2}4f_{5/2}nl_j$		Zn-like ions $3d^{10}nl_j$-$3d^9_{3/2}4f_{5/2}nl_j3d^{10}nl_jn'l'_{j'}$-$3d^9_{3/2}4f_{5/2}nl_jn'l'_{j'}$	
nl_j	mean wavelengths	$nl_jn'l'_{j'}$	mean wavelength
$4s$	5.945(5)	$4s^2$	5.985(0)
$4p_j$	<u>5.943</u>(10),5.949(11)	$4s4p_j$	5.983(8),5.988(6)
$4d_j$	5.947(13),5.951(39)	$4s4d_j$	5.987(13),5.990(38)
$4f_j$	5.946(17),<u>5.951</u>(37)	$4s4f_j$	5.985(17),5.991(36)
		$4p_j4p_{j'}$	<u>5.981</u>(14),5.987(16),5.992(0)
		$4p_j4d_{j'}$	5.985(17),5.988(41),5.990(16),5.994(40)
		$4p_j4f_{j'}$	5.984(20),5.989(19),5.989(39),5.994(39)
		$4d_j4d_{j'}$	5.989(16),5.992(41),<u>5.996</u>(45)
		$4d_j4f_{j'}$	5.988(21),5.991(42),5.993(38),5.996(54)
		$4f_j4f_{j'}$	5.986(21),5.991(41),5.996(45)

relevant to the $3d_{3/2}$-$4f_{5/2}$ transition are much broader. They are considered in Sec. V C.

Now, the preceding description of the possible subarrays is not the proof that they appear in the observed spectrum. A model is needed for explaining how their upper configurations are populated. The most exact scheme is that where the detailed balance of the microscopic processes is computed for each level. However, there exist many processes and an enormous number of levels. For that reason, in the following, we propose the consideration of each configuration or subconfiguration as a whole, and study here only one essential process which populates the levels lying above the ionization limit, the dielectronic recombination.

IV. CALCULATIONS

The basic equations for the process of dielectronic recombination can be found in the book by Cowan.[13] In the present section, formulas are given for treating configurations or subconfigurations as a whole. Then, the numerical *ab initio* calculations in the relativistic parametric central-field model are described.

A. Autoionization rate coefficients

The *state* $J'M'$ of the *energy level* J' of an initial configuration C' belonging to the $(N+1)$-electron ion enters the autoionization process

$$(N+1)J'M' \rightarrow (N)JM + \varepsilon l_0 j_0 m_0 \ .$$

This represents a nonradiative transition to the state JM of the configuration C of the N-electron ion, leaving an outcoming electron, characterized by its kinetic energy ε, its orbital momentum l_0, and its total angular momentum j_0 with projection m_0. The autoionization transition probability of the state $J'M'$ towards the state JM reads, in the isolated-resonance approximation,

$$A^a_{J'M' \rightarrow JM} = (2\pi/\hbar) \sum_{l_0, j_0, m_0} |(JM, l_0 j_0 m_0 | G | J'M')|^2 \ . \tag{1}$$

In general, the matrix element in the right-hand side of (1) involves the total Hamiltonian H for the ion with $(N+1)$ electrons. However, in the central-field approximation, the wave functions of all the electrons belonging to the state M and to the state M', and of the outcoming electron, are solutions of the same monoelectronic Hamiltonian. As a result, H can be restricted to the electrostatic interaction G. Furthermore, the kinetic energy ε of the outcoming electron is deduced from the energy-conservation law

$$E(J) + \varepsilon = E(J') \ . \tag{2}$$

The decrease in time of the population $n_{J'M'}$ of the state $J'M'$ due to autoionization leaving the N-electron ion in the state JM is governed by the rate equation

$$dn^a_{J'M' \rightarrow JM} = -n_{J'M'} A^a_{J'M' \rightarrow JM} dt \ . \tag{3}$$

By summation over M, one obtains the autoionization probability $A^a_{J'M' \rightarrow J}$ from the initial state $J'M'$ towards all the states of the final level J. This coefficient does not depend on the M' value of the initial state. Supposing that, for the $g_{J'} = 2J'+1$ states, $n_{J'M'}$ does not depend on M' (all the states belonging to the same level are equally populated), and summing Eq. (3) over M', one obtains the autoionization rate $A^a_{J' \rightarrow J}$ from the level J' to the level J. This coefficient satisfies

$$A^a_{J' \rightarrow J} = A^a_{J'M' \rightarrow J} \tag{4}$$

with

$$dn^a_{J' \rightarrow J} = -n_{J'} A^a_{J' \rightarrow J} dt, \quad n_{J'} = g_{J'} n_{J'M'} \ .$$

This quantity can be summed in two ways for replacing the level-by-level description by another one in terms of configurations or subconfigurations.

(i) If it is chosen to consider the average coefficient $A^a_{SC' \rightarrow C}$ describing the autoionization of all the states $J'M'$ of the subconfiguration SC' towards all the states JM of the configuration C, Eq. (3) is summed over JM and $J'M'$. If one assumes that all the $g_{SC'}$ states of SC' are equally populated, the evolution with time of the population $n_{SC'}$ of the subconfiguration SC' is determined by

$$dn^a_{SC'\to C} = -n_{SC'} A^a_{SC'\to C} dt \ , \tag{5}$$

with

$$g_{SC'} A^a_{SC'\to C} = \sum_{J'\in SC'} \sum_{J\in C} g_{J'} A^a_{J'\to J} = (2\pi/\hbar) Q_{SC'\to C} \ . \tag{6}$$

(ii) If the average is computed over the whole configuration C', Eqs. (5) and (6) are replaced by

$$dn^a_{C'\to C} = -n_{C'} A^a_{C'\to C} dt \ , \tag{7}$$

and

$$\begin{aligned} g_{C'} A^a_{C'\to C} &= \sum_{SC'} g_{SC'} A^a_{SC'\to C} = \sum_{J'\in C'} \sum_{J\in C} g_{J'} A^a_{J'\to J} \\ &= \sum_{J'M'} \sum_{JM} \sum_{l_0, j_0, m_0} (2\pi/\hbar) |(JM, l_0 j_0 m_0 | G | J'M')|^2 \\ &= (2\pi/\hbar) Q_{C'\to C} \ . \end{aligned} \tag{8}$$

B. Attachment rate coefficients

The inverse process of autoionization is the capture process. With the same notations as in Sec. IV A, it reads

$$(N)JM + \varepsilon l_0 j_0 m_0 \to (N+1) J'M' \ .$$

By summing over all the M' values for the final state and over all the angular quantum numbers $l_0 j_0 m_0$ of the incoming electron, one obtains the attachment rate coefficient $\beta^d_{JM\to J'}(T)$, which does not depend on M, and which is related to the decrease in the population n_J of the level J due to the attachment process

$$dn^d_{J\to J'} = -n_J n_e \beta^d_{JM\to J'}(T) dt \ . \tag{9}$$

The free electrons, with uniform density n_e, are assumed to obey a Maxwellian velocity distribution at the electron temperature T.

The principle of detailed balance allows the evaluation of the attachment rate coefficient from the level J towards the level J' in terms of the autoionization probability $A^a_{J'M'\to J}$

$$\begin{aligned} \beta^d_{JM\to J'}(T) = (h^3/2)(2\pi mkT)^{-3/2} (g_{J'}/g_J) A^a_{J'M'\to J} \\ \times \exp(-\varepsilon/kT) \ , \end{aligned} \tag{10}$$

where m is the electron mass and h and k the Planck and Boltzmann constants; $g_{J'}$ and g_J are the degeneracies of the levels J' and J. When the temperature T and the kinetic energy ε are expressed in electron volts, and the coefficients A^a and β^d in s^{-1} and $cm^3 s^{-1}$, respectively, one obtains

$$\begin{aligned} \beta^d_{JM\to J'}(T) = 1.656\,43\times 10^{-22} T^{-3/2} (g_{J'}/g_J) \\ \times A^a_{J'M'\to J} \exp(-\varepsilon/T) \ . \end{aligned} \tag{11}$$

As in Sec. IV A, the quantity $\beta^d_{JM\to J'}(T)$ deduced from the level-to-level equilibrium can be summed in two ways, for a description in terms of configurations or subconfigurations. In these summations, one assumes that the kinetic energy of the captured electron does not depend on the J' level of the C' configuration, and that all the states of the subconfiguration SC' or of the configuration C' are equally populated.

The coefficient $\beta^d_{C\to SC'}(T)$ is defined through the decrease in the population of the configuration C due to the attachment process leading to an ion in the subconfiguration SC',

$$dn^d_{C\to SC'} = -n_C n_e \beta^d_{C\to SC'}(T) dt \ , \tag{12}$$

with

$$\begin{aligned} \beta^d_{C\to SC'}(T) = (h^3/2)(2\pi mkT)^{-3/2} (g_{SC'}/g_C) \\ \times A^a_{SC'\to C} \exp(-\varepsilon/kT) \ . \end{aligned} \tag{13}$$

Similarly, the attachment coefficient $\beta^d_{C\to C'}(T)$ from the configuration C towards all the states of the configuration C' is

$$\beta^d_{C\to C'}(T) = \sum_{SC'} \beta^d_{C\to SC'}(T) \ . \tag{14}$$

It is proportional to $g_{C'} A^a_{C'\to C}$, as it can be shown from Eq. (8), and it occurs in the time evolution

$$dn^d_{C\to C'} = -n_e n_C \beta^d_{C\to C'}(T) dt \ . \tag{15}$$

C. Population equilibrium in the states of the excited SC' subconfiguration or C' configuration

In the present paper, we assume that the autoionizing levels J' of the $(N+1)$-electron ion are populated only through the attachment of one electron in the ground-state configuration C of the N-electron ion. The population of this J' level can decrease either through autoionization leading to a level J of the N-electron ion, or through radiative decay to some lower level J'' of the $(N+1)$-electron ion, with the probability $A^r_{J'\to J''}$. Only electric dipole transitions are considered. Therefore

$$g_{J'} A^r_{J'\to J''} = (64\pi^4 e^2/3h) \sigma^3 S_{J'\to J''} \ , \tag{16}$$

where σ is the wave number of the transition and $S_{J'\to J''}$ the line strength.[13] As above, the quantity $A^r_{J'\to J''}$ can be summed in two ways for replacing the level-by-level description by another one in terms of configurations[10] or subconfigurations.[5]

By neglecting the changes of the wave numbers σ be-

tween the different transitions in the array, and by supposing that all the states of the upper configuration are equally populated, one can express the radiative decay from the configuration C' to the configuration C'' by

$$dn^r_{C'\to C''} = -n_{C'} A^r_{C'\to C''} dt \ , \tag{17}$$

where

$$g_{C'} A^r_{C'\to C''} = (64\pi^4 e^2/3h)\sigma^3 S_{C'\to C''} \ . \tag{18}$$

Similarly, for subconfigurations, one writes

$$dn^r_{SC'\to SC''} = -n_{SC'} A^r_{SC'\to SC''} dt \ , \tag{19}$$

where

$$g_{SC'} A^r_{SC'\to SC''} = (64\pi^4 e^2/3h)\sigma^3 S_{SC'\to SC''} \ . \tag{20}$$

From Eqs. (18) and (20), it can be shown that

$$g_{C'} A^r_{C'\to C''} = \sum_{SC'} \sum_{SC''} g_{SC'} A^r_{SC'\to SC''} \ . \tag{21}$$

The intensity of a stabilizing transition $J'\to J''$ is proportional to the population $n_{J'}$ in the initial level. This population results from the equilibrium between the different elementary processes: attachment, autoionization, radiative decay, and collisional population or depopulation of the level. The variations associated with the latter two processes are denoted dn^c_p and dn^c_d respectively. At equilibrium, for each level J'

$$\sum_{J''} dn^c_{pJ''\to J'} + dn^d_{J\to J'} = dn^a_{J'\to J} + \sum_{J''} dn^r_{J'\to J''} + \sum_{J''} dn^c_{dJ'\to J''} \ . \tag{22}$$

In the present paper we do not explicitly calculate the collisional cross sections. We only assume that the collisional processes are sufficiently efficient for ensuring equal populations, either (i) of all the states of the configuration C', or only (ii) of all the states of the subconfiguration SC'. Then, the collisional effects can be deleted from Eq. (22). In case (i), it can be deduced, by summing Eq. (22) over all the levels J' of the configuration C', that the population of each state is given by

$$N_{C'} = n_e n_C (h^3/2)(2\pi mkT)^{-3/2}(1/g_C)(2\pi/\hbar) \times Q_{C\to C'} \exp(-\varepsilon/kT) \times \left[(64\pi^4 e^2/3h) \sum_{C''} \sigma''^3 S_{C'\to C''} + (2\pi/\hbar) Q_{C\to C'} \right]^{-1} \ . \tag{23}$$

Similarly, in case (ii), one obtains the same equation with C' and C'' replaced by SC' and SC''.

In the present paper, the C' configuration is of the type $3d^9 n'fnl$ with $n'=4$ or 5. The most intense radiative decays involve configurations of the type $3d^{10}nl$ (denoted C'' in Sec. IV F) or $3d^{10}n'f$ (denoted C''); indeed these transitions filling the $n=3$ shell have large wave numbers and, therefore, they correspond to large radiative decay rates. But the effects of radiative cascades are neglected. The $3d^{10}n'f$-$3d^9 n'fnl$ array, which is allowed when $l=1$ or 3, is taken into account in the population at equilibrium.

D. Intensities of the subarrays

We are now interested in the analysis of the intensities $I^{n'}_{nlj}$ of the subarrays $3d^{10}nl_j$-$3d^9_{3/2}n'f_{5/2}nl_j$ with $n'=4$ and 5. For given n' and nlj, $A^r_{SC'\to SC''}(n',nlj)$ denotes the corresponding decay rate [Eq. (20)]. The intensity of the subarray is written

$$I^{n'}_{nlj} = N_{n'} g_{SC'} A^r_{SC'\to SC''}(n',nlj) \ , \tag{24}$$

where $N_{n'}$, the population of each state of the subconfiguration SC', is given by either $N_{n'}=N_{C'}$, if one assumes that the collisional effects equilibrate the populations of all the states of the configuration C' [Eq. (23)] or $N_{n'}=N_{SC'}$ if one assumes that the populations of the states are only equilibrated in the subconfiguration SC'.

For the Cu-like case, all the subarrays associated with the same (n,n') pair have the same average energy (Sec. III B). Thus, the intensity of the corresponding peak reads

$$I^{n'}_n = \sum_{lj} I^{n'}_{nlj} \ . \tag{25}$$

E. Autoionization and radiative coefficients

The autoionization coefficients $Q_{SC'\to C}$ and $Q_{C'\to C}$ defined in Sec. IV A [Eqs. (6) and (8)] introduce a summation over the angular quantum numbers $JM, J'M'$, and $l_0 j_0 m_0$. The first case presented here is that where C is built with complete subshells. The notation is $C=nl^{4l+2}$ and $C'=nl^{4l+1}n'l'n''l''$ (in the following, the principal quantum numbers n, n', and n'', which are not relevant in the angular calculations, are often considered as implicit). The configuration C only contains one state, therefore the sum over C can be deleted. The explicit angular results can be obtained through Racah's methods.[14] They are given, for case (i), in the following. (1) For $l'j'\neq l''j''$

$$Q_{SC'\to C}=(2j+1)(2j'+1)(2j''+1)(2l+1)$$
$$\times\left[\sum_{l_0,k}(2l_0+1)\frac{(2l'+1)}{(2k+1)}\begin{bmatrix}l&k&l'\\0&0&0\end{bmatrix}^2\begin{bmatrix}l_0&k&l''\\0&0&0\end{bmatrix}^2\begin{Bmatrix}j&k&j'\\l'&s&l\end{Bmatrix}^2[R^k(jl_0,j'j'')]^2\right.$$
$$+\sum_{l_0,k}(2l_0+1)\frac{(2l''+1)}{(2k+1)}\begin{bmatrix}l&k&l''\\0&0&0\end{bmatrix}^2\begin{bmatrix}l_0&k&l'\\0&0&0\end{bmatrix}^2\begin{Bmatrix}j&k&j''\\l''&s&l\end{Bmatrix}^2[R^k(jl_0,j''j')]^2$$
$$+\sum_{l_0,k,k'}2(2l_0+1)(2l'+1)(2l''+1)\begin{bmatrix}l&k&l'\\0&0&0\end{bmatrix}\begin{bmatrix}l&k'&l''\\0&0&0\end{bmatrix}\begin{bmatrix}l_0&k&l''\\0&0&0\end{bmatrix}\begin{bmatrix}l_0&k'&l'\\0&0&0\end{bmatrix}$$
$$\left.\times\begin{Bmatrix}j&k&j'\\l'&s&l\end{Bmatrix}\begin{Bmatrix}j&k'&j''\\l''&s&l\end{Bmatrix}\begin{Bmatrix}j''&s&l''\\k'&l'&l_0\\j&j'&k\end{Bmatrix}R^k(jl_0,j'j'')R^{k'}(jl_0,j''j')\right], \tag{26}$$

where $s=\frac{1}{2}$ and the R^k integrals are relativistic Slater integrals averaged, for $l_0\neq 0$, over the j_0 values of the incoming electron,

$$R^k(jl_0,j'j'')=\frac{l_0}{(2l_0+1)}R^k(nlj\varepsilon l_0(l_0-s),n'l'j'n''l''j'')+\frac{(l_0+1)}{(2l_0+1)}R^k(nlj\varepsilon l_0(l_0+s),n'l'j'n''l''j'') . \tag{27}$$

(2) For $l'j'\equiv l''j''$, $Q_{SC'\to C}$ reads

$$Q_{SC'\to C}=(2j+1)(2j'+1)^2(2l+1)(2l'+1)^2$$
$$\times\sum_{l_0,k}(2l_0+1)\begin{bmatrix}l&k&l'\\0&0&0\end{bmatrix}^2\begin{bmatrix}l_0&k&l'\\0&0&0\end{bmatrix}^2\begin{Bmatrix}j&k&j'\\l'&s&l\end{Bmatrix}^2\left[\frac{1}{(2k+1)(2l'+1)}-\begin{Bmatrix}j'&s&l'\\k&l'&l_0\\j&j'&k\end{Bmatrix}\right][R^k(jl_0,j'j')]^2 . \tag{28}$$

A similar formula in case (ii) reads

$$Q_{C'\to C}=4(2l+1)(2l'+1)(2l''+1)[1-\delta(n'l',n''l'')/2]$$
$$\times\left[\sum_{l_0,k}\frac{(2l_0+1)}{(2k+1)}\begin{bmatrix}l&k&l'\\0&0&0\end{bmatrix}^2\begin{bmatrix}l_0&k&l''\\0&0&0\end{bmatrix}^2[R^k(ll_0,l'l'')]^2\right.$$
$$+\sum_{l_0,k}\frac{(2l_0+1)}{(2k+1)}\begin{bmatrix}l&k&l''\\0&0&0\end{bmatrix}^2\begin{bmatrix}l_0&k&l'\\0&0&0\end{bmatrix}^2[R^k(ll_0,l''l')]^2$$
$$+\sum_{l_0,k,k'}(-1)^{k+k'+1}(2l_0+1)\begin{Bmatrix}l''&l&k'\\l'&l_0&k\end{Bmatrix}\begin{bmatrix}l&k&l'\\0&0&0\end{bmatrix}\begin{bmatrix}l&k'&l''\\0&0&0\end{bmatrix}$$
$$\left.\times\begin{bmatrix}l_0&k&l''\\0&0&0\end{bmatrix}\begin{bmatrix}l_0&k'&l'\\0&0&0\end{bmatrix}R^k(ll_0,l'l'')R^{k'}(ll_0,l''l')\right| . \tag{29}$$

However, $Q_{C'\to C}$ represents the total autoionization coefficient between the C and C' configurations. For computing numerically $Q_{C'\to C}$ the relativistic Slater integrals $R^k(jl_0,j'j'')$ are replaced by $R^k(jl_0,j'l'')$, i.e., their averages over the j'' value, in the same way as in Eq. (27).

In order to obtain the relativistic dipolar or Slater radial integrals, relativistic orbitals have been determined numerically. They are solutions of the Dirac equation describing the motion of a relativistic electron in the central potential created by the N-electron ion and are obtained through the parametric potential method. The discrete orbitals nlj, $n'l'j'$, and $n''l''j''$ are normalized to unity. The continuum orbitals are normalized to satisfy

$$\int_0^\infty P_{\varepsilon l_0 j_0} P_{\varepsilon' l_0 j_0} dr = \pi\delta(\varepsilon - \varepsilon') ,$$

where the energy ε of the continuum electron is referred to the ionization limit of the N-electron ion, and is expressed in Rydberg units.

F. Numerical results for the dielectronic recombination coefficients

The dielectronic recombination populates the upper levels of the stabilizing transition subarray $3d^{10}nl_j - 3d^9_{3/2}n'f_{5/2}nl_j$ ($n'=4,5$). Its rate coefficient, denoted $\alpha^{n'}_{nlj}(T)$, is directly related to the intensity of the subarray

$$I^{n'}_{nlj} = n_e n_C \alpha^{n'}_{nlj}(T) . \tag{30}$$

As described above, the α coefficient is not calculated in a detailed level-by-level description of the attachment and stabilization process, but in a global description in terms of configurations or subconfigurations, leading to the formula

$$\alpha^{n'}_{nlj}(T; C \to C' \to \mathrm{SC}'') = (h^3/2)(2\pi mkT)^{-3/2}(1/g_C) \times \exp(-\varepsilon_{nl}/kT) A^a_{C' \to C} \times \frac{g_{\mathrm{SC}'} A^r_{\mathrm{SC}' \to \mathrm{SC}''}}{A^a_{C' \to C} + A^r_{C' \to C''} + A^r_{C' \to C'''}} , \tag{31}$$

and to a second formula for $\alpha^{n'}_{nlj}(T; C \to \mathrm{SC}' \to \mathrm{SC}'')$, deduced from Eq. (31) through the replacement of C', C'', C''', and ε_{nl} by SC', SC'', SC''', and ε_{nlj}.

The third term in the denominator of Eq. (31) stands for the alternative radiative decay channel $3d^{10}n'f$-$3d^9n'fnl$ between the C' and C''' configurations (or between SC' and SC''' in the second formula). The quantities ε_{nl} and ε_{nlj} represent, respectively, the kinetic energy of the electron involved in the attachment process leading to the configuration C' or to the subconfiguration SC'.

The autoionizing configurations included in the present work are $3d^94fnl$ with $4 \le n \le 7$ and $3d^95fnl$ with $4 \le n \le 5$. These configurations of the Cu-like ion have an energy lower than that of the first excited configuration $3d^94s$ of the Ni-like ion; thus they cannot autoionize toward it. It also appears in Fig. 3 that the lowest two (for $l=0,1$) cannot autoionize at all.

The autoionization probability and the radiative transition probabilities have been calculated for all these configurations and subconfigurations. The numerical values obtained for the $3d^94fnl$ configurations are reported in Table II. It appears that the radiative decay rate for $3d^{10}nl$-$3d^94fnl$ is nearly n independent, whereas the autoionization rate for $3d^{10}$-$3d^94fnl$ decreases approximately as n^{-3}. For $n=4$ and 5, the autoionization and radiative rates are of the same order of magnitude, and the radiative decay becomes predominant with increasing n.

The corresponding dielectronic recombination (DR) coefficients have been deduced for the electron temperature $100 \le T \le 1500$ eV. The results obtained in the assumption that the collisional processes impose statistically equilibrated populations either (i) in a subconfiguration or (ii) in a whole configuration do not differ significantly.

TABLE II. Autoionizing rates and radiative decay rates relative to the upper configurations of the Cu-like ions. The numbers in parentheses denote powers of 10.

Upper configuration $C'=3d^94fnl$	Autoionization rate: $g_{C'}A^a_{C' \to C}$ $C=3d^{10}$ (s^{-1})	Radiative decay rate: $g_{C'}A^r_{C' \to C''}$ $C''=3d^{10}nl$ (s^{-1})	Radiative decay rate: $g_{C'}A^r_{C' \to C'''}$ $C'''=3d^{10}4f$ (s^{-1})
$3d^94f4d$	2.12(16)	1.32(16)	
$3d^94f^2$	3.02(16)	1.72(16)	
$3d^94f5s$	0.48(15)	2.68(15)	
$3d^94f5p$	0.44(15)	8.03(15)	0.20(15)
$3d^94f5d$	0.64(16)	1.34(16)	
$3d^94f5f$	2.07(16)	1.87(16)	0.79(16)
$3d^94f5g$	0.80(16)	2.41(16)	
$3d^94f6s$	0.25(15)	2.69(15)	
$3d^94f6p$	0.25(15)	8.07(15)	0.10(15)
$3d^94f6d$	0.30(16)	1.34(16)	
$3d^94f6f$	1.01(16)	1.88(16)	0.41(16)
$3d^94f6g$	0.57(16)	2.42(16)	
$3d^94f6h$	0.11(16)	2.96(16)	
$3d^94f7s$	0.15(15)	2.69(15)	
$3d^94f7p$	0.15(15)	8.08(15)	0.06(15)
$3d^94f7d$	0.17(16)	1.35(16)	
$3d^94f7f$	0.58(16)	1.89(16)	0.24(16)
$3d^94f7g$	0.38(16)	2.42(16)	
$3d^94f7h$	0.11(16)	2.96(16)	
$3d^94f7i$	0.01(16)	3.50(16)	

All the subarrays in the Cu-like ion associated with the same (n,n') pair have the same average energy. Thus the quantity

$$\alpha_n^{n'}(T)=\sum_{lj}\alpha_{nlj}^{n'}(T) \tag{32}$$

represents the total DR rate corresponding to all intermediate configurations $3d^9n'fnl$. The variation of $\alpha_n^{n'}(T)$ versus the temperature is reported in Fig. 4, for both assumptions (i) and (ii) above. This variation is very similar to that obtained by Chen for Ni-like gadolinium,[15] in a level-by-level description of the DR process, accounting for configuration-mixing effects.

V. COMPARISON WITH EXPERIMENT

The comparison with experiment is now focused on two characteristic features of the spectra: (i) the position of some satellite peaks, not assigned until now, and their relative intensities, and (ii) the pseudocontinuum structure on the long-wavelength side of the Zn-like peaks.

A. Positions of the peaks

The assignment can already be made with the simple assumption that only the configurations of Ta^{q+} populated directly by dielectronic attachment on the *ground-state* configuration of $Ta^{(q+1)+}$ decay radiatively. For the $3d$-$4f$ transition, these configurations are denoted $3d^94fnl$, $3d^94f4snl$, $3d^94f4s^2nl$, and $3d^94f4s^24pnl$ in the Cu-, Zn-, Ga-, and Ge-like spectra. In Fig. 2, the corresponding emission peaks are marked by two grids. The upper grid $(B-E)$ refers to Cu- through Ge-like peaks where the spectator electrons belong to the $n=4$ shell, and the lower grid $(b-e)$ to the similar peaks where one of the spectator electrons is in the $n=5$ shell. On the left, the peak marked A corresponds to $3d^{10}$-$3d^94f$ in the Ni-like spectrum.

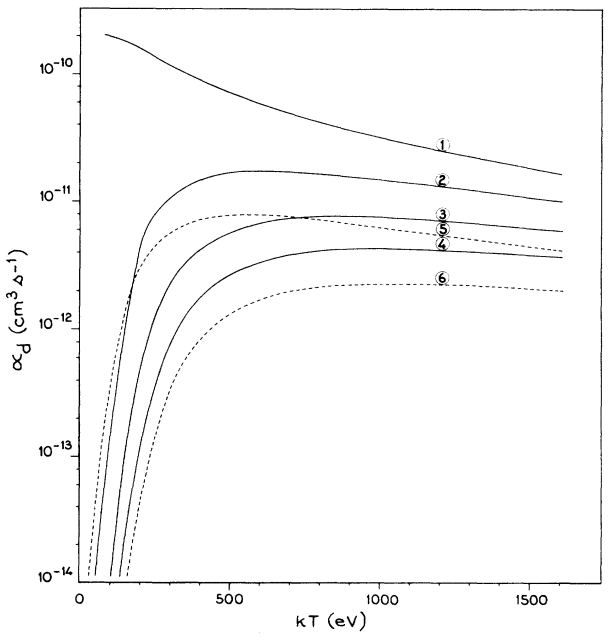

FIG. 4. Dielectronic recombination coefficients α_d as a function of the electronic temperature. Solid curves: 1, $3d^94f4l$; 2, $3d^94f5l$; 3, $3d^94f6l$; 4, $3d^94f\,7l$. Dashed curves: 5, $3d^95f4l$; 6, $3d^95f5l$.

The wavelengths of the peaks are listed in Table III, together with the FWHM. All numbers are computed in the SOSA model,[5] for the $3d_{3/2}$-$4f_{5/2}$ subarrays, and they have been shifted by 0.015 Å (see Sec. III A). The peaks b and c have never before been assigned. They are also clearly apparent in Fig. 1 of the paper by Klapisch *et al.*,[8] and in Fig. 1 of the present paper. The peaks of Ta^{q+} with spectators $n\geq 6$ which are given in Table III merge into that of $Ta^{(q-1)+}$ with $n=4$; for example, those for Cu-like appear as a shoulder between peaks A and b.

B. Relative intensities of the Cu-like peaks

The intensities of three Cu-like peaks can be evaluated in Figs. 1 and 2. They are denoted, respectively,

$$4f(4)=3d^{10}4l\text{-}(3d^9)_{3/2}4f_{5/2}4l$$

(peak B in Fig. 2),

$$4f(5)=3d^{10}5l\text{-}(3d^9)_{3/2}4f_{5/2}5l$$

(peak b), and

$$5f(4)=3d^{10}4l\text{-}(3d^9)_{3/2}5f_{5/2}4l$$

(the farthest Cu-like peak to the left of Fig. 1(a); see also Fig. 1 of Ref. 2, where it is labeled B). Their experimental intensities can now be compared with those computed by means of any of three DR models developed above (Sec. IV), or by means of the simple local-thermodynamic-equilibrium (LTE) assumption.

The case of the first peak is complex, because the $3d^94f4s$ and $3d^94f4p$ configurations cannot be populated through attachement, as they are two low in the energy

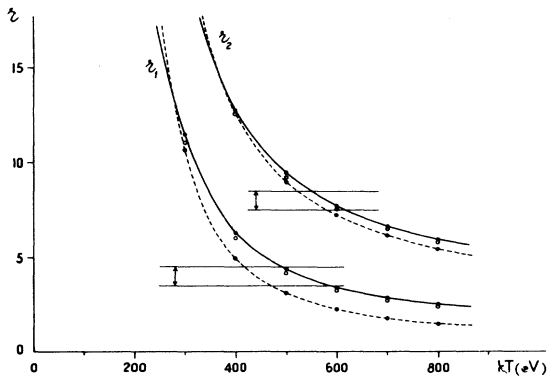

FIG. 5. Intensity ratios $r_1=I[4f(4)]/I[4f(5)]$ and $r_2=I[4f(4)]/I[5f(4)]$ in the Cu-like spectrum, as functions of the electronic temperature. Solid curves: in the calculations, the averages are taken on subconfigurations [(i) in Sec. IV A]. Circles: the averages are taken on configurations [(ii) in Sec. IV A]. The experimental values are $r_1=4\pm0.5$ and $r_2=8\pm0.5$. Their limits are represented by the horizontal bars.

TABLE III. Mean wavelengths and widths of the different peaks of the $3d_{3/2}$-$4f_{5/2}$ transitions (in Å and mÅ), calculated by taking into account only the subarrays arising from subconfigurations *directly populated by dielectronic recombination* from the ground-state level of the preceding ionic species. *A*, *B*, *C*, *D*, *E*, *b*, *c*, *d*, and *e* are the labels of the peaks on Fig. 3. The instrumental width (0.006 Å) is taken into account in the calculation of the widths. bl stands for blended.

	$n=4$	$n=5$	$n=6$	$n=7$
Cu-like:				
$3d^{10}nl$-$3d^9 4fnl$				
Calc.	5.947[14]	5.920[10]	5.912[8]	5.909[7]
Expt.	5.946	5.919	bl *A*	bl *A*
	(peak *B*)	(peak *b*)		
Zn-like:				
$3d^{10}4snl$-$3d^9 4f4snl$				
Calc.	5.985(20)	5.957(13)	5.950	
Expt.	5.983	5.957	bl *B*	
	(peak *C*)	(peak *c*)		
Ga-like:				
$3d^{10}4s^2nl$-$3d^9 4f4s^2nl$				
Calc.	6.021(17)	5.994(11)	5.986	
Expt.	6.021	5.994	bl *C*	
	(peak *D*)	(peak *d*)		
Ge-like:				
$3d^{10}4s^2 4pnl$-$3d^9 4f4s^2 4pnl$				
Calc.	6.059(24)	6.032(18)		
Expt.	6.057	6.033		
	(peak *E*)	(peak *e*)		

spectrum. The yields of alternative mechanisms must be examined.

(i) The collisional excitations (CE) from $3d^{10}4s,4p$ to $3d^9 4f4s,4p$ can be estimated by using Van Regemorter's equation (22),[16] which relates them to the corresponding $3d^{10}4s,4p - 3d^9 4f4s,4p$ radiative electric dipole ($E1$) transition probabilities. The Saha formula is also needed for linking, at $T \approx 500$ eV and $n_e \approx 10^{22}$ cm^{-3}, the population of the ground-state level of $3d^{10}4s,4p$ to that of $3d^{10}$, as the latter is the initial level in the DR processes which populate $3d^9 4f4d$ and $3d^9 4f^2$. At equilibrium between CE from $3d^{10}4s,4p$ and radiative decay towards it, the obtained population per state in $3d^9 4f4s,4p$ is nearly two orders of magnitude smaller than that produced in $3d^9 4f4d$ through the attachment process (see Table II).

(ii) The collisional deexcitation (CD) from $(3d^9)_{3/2}4f_{5/2}4d$ to $3d^9_{3/2}4f_{5/2}4p$ can be evaluated in an analogous way, and compared to the $E1$ process from $3d^9_{3/2}4f_{5/2}4d$ to $3d^{10}4d$. The result is that the total CD yield is about eight times smaller than the $E1$ yield. However, it is known that Van Regemorter's formula underestimates the CD and CE yields in the case of intrashell transitions, like 4*p*-4*d*, and also in the case of heavy ions.[17]

Therefore it can be assumed that the populations built in both excited configurations $3d^9 4f4d$ and $3d^9 4f^2$ through dielectronic recombination are distributed over the close configurations, i.e., mainly, all the others having pairs of external electrons in the $n=4$ shell. Now, among the latter configurations, there are two which contribute to the 3*d*-4*f* emission (those with external pairs $4f4s$ and $4f4p$), three which contribute to 3*d*-4*p* (those with $4p4s$, $4p^2$, and $4p4d$), and three which are nearly metastable (those with $4s^2$,$4s4d$, and $4d^2$). The radiative branching ratio is largely in favor of the 3*d*-4*f* over the 3*d*-4*f* transitions, as is shown by the oscillator strength (gf) calculations in Au^{52+} through Au^{48+} published by Busquet *et al.*[7] Then, through this redistribution, only the $3d^9 4f4s$ and $3d^9 4f4p$ are populated, in the first approximation. It is concluded that this effect does not change very much the total intensity of any 3*d*-4*f* peak: this comes from the fact that the strengths of the $3d^{10}4l_j$-$3d^9_{3/2}4f_{5/2}4l_j$ subarrays are proportional to the $2j+1$ degeneracy[5] (except for the single case $l_j = f_{5/2}$), and that their average wavelengths are nearly equal.

The intensity ratios

$$r_1 = I[4f(4)]/I(4f(5)]$$

and

$$r_2 = I[4f(4)]/I(5f(4)] ,$$

derived through Eq. (30)–(32) for the three peaks studied in the present section, do not depend, in the DR model, on n_e or on the $3d^{10}$ density population. Their variations versus kT are represented in Fig. 5 by solid lines. The experimental values are $r_1 = 4 \pm 0.5$ and $r_2 = 8 \pm 0.5$. It is clear from Fig. 5 that kT values between 550 and 600 eV can lead to computed results for r_1 and r_2 which both agree with experiment, but these values certainly overestimate the true temperatures, because of the approximations made in the preceding argument. In contrast, the LTE results, represented by dashed lines in the same figure, do not fit both experimental values for any temperature.

C. Pseudocontinuum shape

The pseudocontinuum shape of the long-wavelength side of the $3d$-$4f$ pattern can be interpreted in the assumption of the collisional redistribution in the upper configurations proposed in Sec. V B. More precisely, electronic collisions are assumed to transfer atoms, from the configurations of Ta^{q+} populated directly by attachment on the ground-state configuration of $Ta^{(q+1)+}$, to the close configurations, i.e., those where only the l quantum numbers of the spectator electrons have been changed. For example, $3d^9 4f 4pnl$ is populated from $3d^9 4f 4snl$. Another mechanism populating many upper configurations in the Zn-like, Ga-like, etc., spectra is the electronic attachment on the low excited configurations like $3d^{10}4s4p$, $3d^{10}4s^2 4d$, etc.

Then, the number of emitted subarrays is greatly increased: 28 in the case of the Zn-like spectrum (they are listed in Table I), 82 for Ga-like, and 196 for Ge-like spectra. In the latter two cases, only some subarrays are listed in Table IV: we present those whose mean wavelengths are minimum and maximum (underlined) and we indicate the mean energy values of the upper configurations. Following the remark written in the Appendix, it can be noted that the difference Δ between the minimum and the maximum mean wavelengths of the different subarrays is proportional to the number of $n=4$ spectator electrons; as can be seen in Table I and Table IV, $\Delta=8$ mÅ in the Cu-like subarrays (peak B), 15 in the Zn-like subarrays (peak C), 23 in the Ga-like subarrays (peak D), 30 in the Ge-like subarrays (peak E), 16 in the Ga-like subarrays (peak d, where one of the spectator electrons is in the $n=5$ shell) and 22 in the Ge-like subarrays (peak e, where one of the spectator electrons is also in the $n=5$ shell). Owing to the great number of subarrays, each of them having a width larger than 10 or 20 mÅ, a quasicontinuity of peaks can be observed from about 5.96 Å towards larger wavelengths. At the bottom of Fig. 2, we have represented the spread of the positions of the subarray corresponding to each kind of transition and it is clear that C, d, D, e, and E constitute a continuous chain of peaks.

Now the question is: why does such a continuum not appear in the $3d$-$5f$ pattern? There are two reasons. On one hand, the upper configurations are about 620 eV higher, and the highest are much less populated; in the Cu-like spectrum, for example, the α coefficients are about eight times smaller for $5f(5)$ than for $5f(4)$, as shown by curves 5 and 6, at $kT=550$ eV, in Fig. 4. On the other hand, the distance between the peaks A, B, C, D, . . . is 32 mÅ in the $3d$-$4f$ transition and 52 mÅ in the $3d$-$5f$ transition (see Table I in Ref. 2). In conclusion the arrays analogous to d and e are very weak, C, D, and E, are narrower and their distance much larger, this

TABLE IV. Mean wavelengths of *some* subarrays corresponding to the $3d_{3/2}$-$4f_{5/2}$ transitions of the Ga- and Ge-like ions. In each case, the shortest and the longest wavelengths are underlined, to show that the arrays C, d, D, e, and E constitute a continuous chain of peaks. The energies of the upper configurations are referred to the ground-state configuration of the relevant ion.

Spectator electrons	Mean wavelength of the subarrays (Å)	Mean value of the energy of the upper configurations (eV)
	Ga-like ions: peak D (three $4l$ spectator electrons)	
$4s4p^2$	6.016,6.022,6.028	2157
$4s4d^2$	6.024,6.027,6.031	2646
$4s4p4d$	6.020,6.024,6.026,6.029	2350
$4p^3$	<u>6.014</u>,6.020,6.026,6.031	2323
$4d^3$	6.026,6.029,6.033,6.036	2897
$4f^3$	6.022,6.027,6.032,<u>6.037</u>	3422
	Ga-like ions: peak d (two $4l$ and one $5l$ spectator electrons)	
$4s4p5s$	5.992,5.997	2908
$4s4p5d$	5.993,5.993,5.999,5.998	3074
$4p^2 5s$	<u>5.990</u>,5.995,6.001	3071
$4p^2 5d$	5.991,5.991,5.997,5.996,6.003,6.002	3236
$4d^2 5s$	5.997,6.001,6.004	3453
$4d^2 5d$	5.999,5.998,6.002,6.002,<u>6.006</u>,6.005	3617
	Ge-like ions: peak E (four $4l$ spectator electrons)	
$4s4p^3$	6.052,6.057,6.063,6.069	2148
$4p^4$	<u>6.049</u>,6.055,6.061	2317
$4d^4$	6.064,6.068,6.072,6.075,<u>6.079</u>	3085
$4f^4$	6.059,6.064,6.069,6.074,6.079	3797
	Ge-like ions: peak e (three $4l$ and one $5l$ spectator electrons)	
$4s^2 4d5s$	6.032,6.036	2927
$4s^2 4d5f$	6.033,6.033,6.037,6.037	3171
$4p^3 5s$	<u>6.024</u>,6.030,6.036,6.042	3051
$4d^3 5s$	6.035,6.039,6.043,<u>6.046</u>	3626

prevents the coalescence of the peaks and there is no continuum (see Fig. 1 of Ref. 2).

D. Comparison of low- and high-irradiance spectra

It is interesting to consider the marked differences between the $3d_{3/2}$-$4f_{5/2}$ patterns in Figs. 1(a) and 1(b). The Cu- and Zn-like satellite features which are denoted *b* and *c* in Fig. 2 appear as shoulders in Fig. 1(a), but as definite peaks in Fig. 1(b); the changes of the intensity ratios A/b and B/c are spectacular.

In the (a) and (b) spectra, both the electronic temperature T and the electronic density n_e are different. The following study concerns, for example, the observed modification of the intensity ratio r of the peaks denoted *A* and *b* in Fig. 2, uncorrected for line opacity effects.

For peak *A*, the average population densities per state in $3d^9 4f$ and $3d^{10}$ can be related through the Boltzmann formula

$$N(3d^9 4f) = N(3d^{10}) \exp\{-[E(3d^9 4f) - E(3d^{10})]/kT\} . \quad (33)$$

For peak *b*, the relevant equation is

$$N(3d^9 4f 5l) = kN(3d^{10}) n_e T^{-3/2} \times \exp\{-[E(3d^9 4f 5l) - E(3d^{10})]/kT\} , \quad (34)$$

which is a consequence of the DR process [Eq. (23)]. In this equation, the quantities referring to $3d^9 4f 5l$ are weighted averages over $l = 0$–4, and the k factor depends on the model used (See Sec. IV), but neither on n_e nor on T. Thus the ratio of the r ratios in Figs. 1(a) and 1(b) reads

$$\frac{r(a)}{r(b)} = \frac{n_e(b)}{n_e(a)} \left[\frac{T(a)}{T(b)} \right]^{3/2} \times \exp\left\{ -[E(3d^9 4f) - E(3d^9 4f 5l)] \times \left[\frac{1}{kT(a)} - \frac{1}{kT(b)} \right] \right\} , \quad (35)$$

in evident notations.

The experimental value for $r(a)/r(b)$ is about 1.6. As we cannot deduce the change in n_e *and* T from only one experimental result, we can only check that the relation between their variations, given by Eq. (35), makes sense. Let us suppose that $T(a) = 500$ and $T(b) = 400$ eV, then $n_e(a)/n_e(b) = 1.55$. If $n_e(a) = 10^{22}$ cm^{-3}, then $n_e(b) = 6.5 \times 10^{21}$ cm^{-3}; both of these values are in the most probable range. They are similar to those reported by Bailey *et al.*[18] in their studies on europium.

The parameters of the plasma in (*b*) are such that the ionic abundances are very different from those in (*a*): The Ni- and Cu-like ions are much less abundant whereas the Ga- and Ge-like ions are much more abundant. Then, the hundreds of subarrays described in Sec. V C for the Ga- and Ge-like $3d$-$4f$ emission have their intensities much increased and they appear, indeed, like a pseudocontinuum.

VI. CONCLUSION

Spectra emitted at short wavelengths by highly ionized heavy ions are very interesting, because they yield information on the hottest parts of the plasma. In the present paper, the interest is focused on the $3d$-$4f$ transitions in the ions Ta^{41+} through Ta^{45+}, in the range 4.5–6 Å, with the following questions. (i) Is the dielectronic recombination the main process responsible for the population of the upper levels of these transitions, which are essentially located above the ionization potential, for all ions? (ii) Where does the pseudocontinuum structure underlying the $3d$-$4f$ pattern come from?

Answers have been given to these questions through *ab initio* calculations carried out for whole configurations and subconfigurations. Such a procedure has been applied for several years to the electric dipole ($E1$) emission process, leading to the concept of transition arrays and subarrays. Here, it is extended to the DR process.

First, the DR results compare nicely with the level-by-level calculations obtained by Chen in Ni-like gadolinium.[15] Secondly, the intensity ratios of two $3d$-$4f$ and one $3d$-$5f$ Cu-like peaks, measured on emission spectra of a laser-produced tantalum plasma, agree with computed values in the temperature assumption $kT \approx 550$ eV. Thirdly, the pseudocontinuum structure is shown to result from the coalescence of hundreds of weak transition subarrays.

It is well known that, at high electronic densities, all the atomic processes build up an equilibrium state approaching LTE. The DR and emission processes studied here are inextricably mingled with others like collisional excitation and deexcitation, and radiative and three-body recombinations. The former two have been estimated, and the latter two have been neglected. The cascade effects from higher levels should be negligible, because

TABLE V. Comparison of the values of the $F^0(3d,4l)$ and $F^0(4f,4l)$ Slater integrals calculated with the hydrogenic assumption and in the central-field model.

	$F^0(3d,4l)$		$F^0(4f,4l)$	
$4l$	Hydrogenic	Central field	Hydrogenic	Central field
$4s$	517 590	623 700	455 096	513 500
$4p$	539 082	617 600	468 282	507 500
$4d$	584 851	631 700	497 292	512 000
$4f$	651 814	662 100	551 167	543 500

levels high enough for having large $E1$ probabilities are weakly populated. The optical thickness has not been taken into account.

In the line of the present work, it would be easy to calculate *ab inito* the DR process in the Zn-, Ga-, and Ge-like spectra, starting from electronic attachment on the ground and lowly excited configurations of the preceding ions.

Now, to improve the present approach, it is necessary to build a collisional-radiative model, including many processes, where the levels will be replaced by configurations or subconfigurations. Thus, quick evaluations of the relative importances of these processes in the dynamical equilibrium of the plasma would be obtained.

APPENDIX: QUASICOINCIDENCE OF THE Cu-LIKE SUBARRAYS

The quasicoincidence of the average wavelengths of the Cu-like subarrays in Table I can be understood by looking at the behavior of hydrogenic radial functions. In the frame of the nonrelativistic central-field model, let the electrostatic repulsion energy be restricted to the F^0 Slater integrals; indeed, for any pair of interacting orbitals in any atomic states, both the value and the angular coefficient of the F^0 integrals are much larger, in absolute value, than those of any other Slater integral.[19] In this approximation, the average energy of the $3d^{10}4l_j$-$3d^9_{3/2}4f_{5/2}4l_j$ subarray is increased, if l is changed into l', by just the quantity

$$\Delta(l,l') = F^0(3d,4l) - F^0(3d,4l') + F^0(4f,4l') - F^0(4f,4l) .$$

Now, in highly ionized atoms like Ta^{44+}, the radial functions can be approximated by their hydrogenic expressions for a suitable effective value of Z, say, 50. The corresponding values of the F^0 integrals can be deduced easily from those published by Butler[20] for $Z=1$. They are listed in Table V together with physical values calculated *ab initio* by means of the relativistic central-field RELAC code[11,12] and reduced to their nonrelativistic approximation.[21] The physical values show the same behavior as the hydrogenic ones. Then, from the hydrogenic values, one derives $\Delta(1,0)=0.0378$, $\Delta(2,1)=0.0764$, and $\Delta(3,2)=0.0596$, in atomic units. These values yield shifts between the energies of the successive subarrays which correspond respectively, for $\lambda=6$ Å, to 3.0, 6.0, and 4.7 mÅ, i.e., smaller than the subarray widths. It can be checked that the contributions of the integrals other than F^0 do not change the order of magnitude of these results. For ions with n spectator electrons, the quantity equivalent to $\Delta(l,l')$ become roughly n times larger; this can be checked in Tables I and IV.

*Permanent address: Lawrence Livermore National Laboratory, Livermore, CA 94550.

[1]N. Tragin, J.-P. Geindre, P. Monier, J.-C. Gauthier, C. Chenais-Popovics, J.-F. Wyart, and C. Bauche-Arnoult, Phys. Scr. **37**, 72 (1988).

[2]P. Audebert, J.-C. Gauthier, J.-P. Geindre, C. Chenais-Popovics, C. Bauche-Arnoult, J. Bauche, M. Klapisch, E. Luc-Koenig, and J.-F. Wyart, Phys. Rev. A **32**, 409 (1985).

[3]C. Bauche-Arnoult, E. Luc-Koenig, J.-F. Wyart, J.-P. Geindre, P. Audebert, P. Monier, J.-C. Gauthier, and C. Chenais-Popovics, Phys. Rev. A **33**, 791 (1986).

[4]A. Zigler, M. Klapisch, and P. Mandelbaum, Phys. Lett. A **117**, 31 (1986).

[5]C. Bauche-Arnoult, J. Bauche, and M. Klapisch, Phys. Rev. A **31**, 2248 (1985).

[6]P. G. Burkhalter, D. J. Nagel, and R. R. Whitlock, Phys. Rev. A **9**, 2331 (1974).

[7]M. Busquet, D. Pain, J. Bauche, and E. Luc-Koenig, Phys. Scr. **31**, 137 (1985).

[8]M. Klapisch, P. Mandelbaum, A. Zigler, C. Bauche-Arnoult, and J. Bauche, Phys. Scr. **34**, 51 (1986).

[9]P. Alaterre, C. Popovics, J.-P. Geindre, and J.-C. Gauthier, Opt. Commun. **49**, 140 (1984).

[10]J. Bauche, C. Bauche-Arnoult, E. Luc-Koenig, and J.-F. Wyart, Phys. Rev. A **28**, 829 (1983).

[11]E. Koenig, Physica (Utrecht) **62**, 393 (1972).

[12]M. Klapisch, J.-L. Schwob, B. S. Fraenkel, and J. Oreg, J. Opt. Soc. Am. **67**, 148 (1977).

[13]R. D. Cowan, *The Theory of Atomic Structure and Spectra* (University of California Press, Berkeley, 1981).

[14]B. R. Judd, *Operator Techniques in Atomic Spectroscopy* (McGraw-Hill, New York, 1963).

[15]M. H. Chen, Phys. Rev. A **35**, 4129 (1987).

[16]H. Van Regemorter, Astrophys. J. **136**, 906 (1962).

[17]O. Bely and H. Van Regemorter, Annu. Rev. Astron. Astrophys. **8**, 329 (1970).

[18]J. Bailey, J. D. Kilkenny, Y. Lee, S. Maxon, J. H. Scofield, and D. Weber, Phys. Rev. A **35**, 2578 (1987).

[19]J. C. Slater, *Quantum Theory of Atomic Structure* (McGraw-Hill, New York, 1960).

[20]P. H. Butler, P. E. H. Minchin, and B. G. Wybourne, At. Data **3**, 153 (1971).

[21]J. Bauche, C. Bauche-Arnoult, E. Luc-Koenig, and M. Klapisch, J. Phys. B **15**, 2325 (1982).